Synthesis of supported ZSM-5 nanoparticles

Olfa Ben Moussa, Ilef Borghol, David Hu, Sandra Casale, Yannick Millot, Celine Sayag, Juliette Blanchard, Olivier Durupthy

Synthesis of supported ZSM-5 nanoparticles

Olfa Ben Moussa,[a,b] Ilef Borghol,[a,b] David Hu [a], Sandra Casale [a], Yannick Millot [a], Céline Sayag [a], Juliette Blanchard[a,*], Olivier Durupthy[b]

[a] *Sorbonne Université, CNRS, Laboratoire de Réactivité de Surface, LRS UMR 7197, F-75005, Paris, France.*

[b] *Sorbonne Université, CNRS, Collège de France, Laboratoire de Chimie de la Matière Condensée de Paris, LCMCP, F-75005, Paris, France*

Abstract

The influence of the support on the nucleation of ZSM-5 nanoparticles has been studied for three supports: γ-alumina, zirconia and carbon nanotubes (CNT). While zeolite nucleation was suppressed in presence of alumina and strongly delayed in presence of zirconia, it occurred without delay in presence of CNT. These differences are explained by the partial dissolution of the support (for alumina and zirconia supports) that modify the composition of the zeolite nucleation solution. For the CNT/zeolite sample, the obtained composite contains about 60 wt% of zeolite and develops a surface area of 776 $m^2.g^{-1}$.

Keyword: Nanozeolites, composites, carbone nanotubes, supported zeolite nanoparticles

Highlights:

-growth of supported ZSM-5 nanoparticles (NPs) is support-dependant.

-γ-Al_2O_3 strongly inhibits the growth of ZSM-5 NPs due to increased Al concentration

-ZrO_2 mildy inhibits the growth of ZSM-5 NPs

-CNT (carbon nanotubes) do not inhibit the growth of ZSM-5 NPs

- a high surface area ZSM-5/CNT composite is formed in presence of CNT

* Corresponding author. Tel.: 33-(0)1 44-27-49-14; fax: 33-(0)1 44-27-60-33; e-mail: juliette.blanchard@sorbonne-universite.fr

1. Introduction

Zeolite nanoparticles (NP, 10-100 nm) are promising alternatives to conventional micrometric zeolite particles for applications in catalysis as their larger external surface area ensure a better diffusion or reactants and products [1-3]. However, their nanometric size makes difficult their recovery and manipulation after catalytic reaction. Furthermore, the tendency of zeolites nanoparticles to aggregate during synthesis and/or upon drying and calcination usually results in a partial loss of external surface area, and as a consequence, reduces the positive impact of their nanometric crystallite size on the diffusion of reactants [4]. Stabilization of zeolite nanoparticles by a support could help preventing their aggregation and facilitate their recovery [5-7]. Moreover, the presence of this additional support could provide an alternative surface for the deposition of an active phase (e.g. metallic nanoparticles) [6, 8]. We recently reported the successful preparation of zeolite-alumina composites by heterocoagulation of zeolite and boehmite nanoparticles [6]. Still, an alternative and very efficient approach would be to directly grow the zeolite nanoparticles on a support. Beside its simplicity this approach could have the added advantage of the pre-existence of a solid-liquid interface that could facilitate the nucleation and results in the formation of zeolite nuclei on the support. While the growth of dense film of zeolite on support has become common [9], the direct growth of zeolite nanoparticles on a support has been scarcely attempted up to now [7, 10, 11]. We report herein for the first time the crystallization of ZSM-5 zeolite nanoparticles in the presence several supports, that have been selected based on their potential as catalyst support and on their high external surface area: γ-alumina, zirconia and carbon nanotubes (CNT). A careful characterization of the obtained materials reveals clear differences in the impact of the presence of support on the crystallization of the zeolite nanoparticles and on the nature of the composite.

2. Materials and methods

2.1. Synthesis of composites materials

Synthesis protocols for the preparation of zeolite nanoparticles were adapted from the procedures developed by Chiang and coworkers [12-14] that allow the synthesis of colloidal ZSM-5 with a high yield (up to 91%).

0.16 g (0.0008 mol) of aluminum isopropoxide (AIP, Sigma-Aldrich) was added to 20 mL of a 1 mol L^{-1} aqueous solution of tetrapropylammonium hydroxide (TPAOH, Sigma-Aldrich). The mixture was stirred until complete dissolution of AIP (ca. 30 min.). 95 mL of water followed by 16.7 g (0.08 mol) of tetraethoxysilane (TEOS) were added to the above solution. The resulting clear solution was aged under stirring during at least 2 h and then evaporated under vacuum (100 mbar, 80 °C, rotary evaporator) in order to remove the isopropanol and ethanol molecules formed by the hydrolysis of AIP and TEOS and to decrease the [H_2O]/[|Si] ratio to 9.5 (corresponding to a SiO_2 concentration of about 20%). The molar composition of the synthesis solution was: ¼ TPAOH : 1/50 Al_2O_3 : 1 SiO_2 : 78 H_2O : 4 EtOH : 6/50 iPrOH before evaporation and : 1/4 TPAOH : 1/50 Al_2O_3 : 1 SiO_2 : 9.5 H_2O after. 10 g of the viscous solution containing the zeolite precursors was then poured in a Duran glass pressure bottle and the desired amount of support (multiwalled CNT, 6-8 walls, prepared by CVD using CoMoCAT, SouthWest NanoTechnologies;Inc., provider Sigma-Aldrich; γ-alumina, Puralox TH100, Sasol; monoclinic zirconia, E101 MEL Chemicals, Manchester, U.K.) was added. For each support, the amount of support to be added to the solution (see Table 1) was estimated based on the external surface area of the support, the geometrical surface of the zeolite NPs and the yield of formation of zeolite under the same conditions, but in absence of support (about 50%), with the objective to have, in the final composite, similar external surfaces provided by the two components.

A reference bottle (containing only the solution of zeolite precursors) was also prepared. The bottles were sealed and heated under stirring (500 rpm) at 65 °C during either 60 h or 100 h in an oven. At the end of the hydrothermal treatment, the solid phase was separated

from the synthesis solution by centrifugation. The speed of centrifugation was adjusted depending on the sample: for the reference suspension (zeolite nanoparticles without support) a high speed centrifugation was required because of the small size and low density of the zeolite nanoparticles; optimized centrifugation protocol is: 57440 g (26000 rpm) during 1 h, after dilution with water (1ml suspension for 9 ml water). For the supported samples a milder centrifugation was used in order to recover only the composite (so that isolated zeolite NPs (if any) remain in the solution): 29000 g (16500 rpm) 10 min. We verified that, under these conditions no sedimentation of the zeolites nanoparticles was observed in the reference suspension.

The solid phase was eventually dried at 60 °C and then calcined in a muffle furnace for 4 h (heating rate 1.5 °C min^{-1}). Calcination temperature was set at 550 °C for all samples except CNT-based composites which have been calcined at 500 °C. This lower calcination temperature was imposed by the onset of thermal decomposition of the CNT under air above 500°C.

The 60 h duration for the hydrothermal treatment corresponds to the time required to reach a yield (estimated on calcined sample and based on Si: number of mol of Si in the calcined sample divided by number of mol of Si introduced during synthesis) of 40-50% for unsupported zeolite nanoparticles.

2.2. Characterization

Crystallinity of materials was investigated using X-ray diffraction (XRD) with a Bruker D8 ADVANCE diffractometer (Cu Kα radiation) over a 2θ range from 4° to 40° with a step size of 0.02° and a counting time of 2 s per step.

Textural properties (total and external surface areas) were obtained from the analysis of N_2-sorption isotherms measured on a BelSorp Max set-up. Prior to the measurement, samples were treated under vacuum at 200 °C during at least 3 h. Total surface area was estimated using the BET model. “External” (non-microporous) surface area was determined based on the

NLDFT simulation of the adsorption isotherm (considering the surface associated with pore larger than 5 nm as "external" surface).

The elemental compositions of (unsupported) zeolite nanoparticles and of the zirconia and alumina composites were determined using X-ray fluorescence analysis (XRF); experiments were conducted under He flow with an energy dispersive spectrometer (XEPOS with Turboquant powder software) equipped with a 50-Watt end-window X-ray tube. Composition of the zeolite-CNT composite was determined by analyzing the TGA curves. Thermogravimetric experiments were performed on a SDTQ 600 apparatus between 30-900 °C. After a plateau at 50 °C, the sample (ca. 30 mg) was heated in air flow (100 mL min^{-1}) with a heating rate of 7 °C min^{-1}.

Samples were also examined using Transmission Electron Microscopy (TEM). Experiments were performed using a JEOL 2010 microscope operating at 200 kV with a LaB6 filament and equipped with an Orius CCD camera (Gatan).

Dynamic light scattering (DLS) experiments were performed on suspensions obtained by dispersing zeolite nanoparticles in water (dilution~ 1 g L^{-1}) and using a Malvern Zetasizer nanoZS90 apparatus.

3. Results

3.1. Unsupported ZSM-5 zeolite nanoparticles

As mentioned in the experimental part, the protocol we developed for the preparation of the composite samples is based on a procedure proposed by Chiang and co-workers for the preparation of colloidal suspensions of ZSM-5 nanoparticles [12-14]. The synthesis conditions optimized by these authors differ by two aspects from the conventional conditions for the crystallization of the ZSM-5: synthesis is performed at considerably higher concentration of silica and at substantially lower temperature. Under these conditions, nucleation of zeolite particles is drastically favored over their growth. These conditions of synthesis have been adapted in order to meet the requirement for the synthesis of composites. More precisely, the

temperature for the hydrothermal treatment has been decreased (from 80°C to 66°C) in order to reduce potential damages to the support during hydrothermal treatment, and slightly higher dilution has been used in order to reduce the viscosity of the solution. In absence of a support, the formation of zeolite nanoparticles under these conditions requires a prolongation of the duration of the hydrothermal treatment, compared to the protocol developed by Chiang and co-workers. A duration of 60 h under stirring allows collecting a fairly high amount of solid phase (yield of 50% based on Si).

The X-Ray diffractogam of the sample (Figure 1, curve (a)) reveals a good crystallinity with no crystalline impurity (ICDD file 01-085-1208). The nanometer size of the zeolite crystallites was ascertained based on XRD (35 nm by applying Scherrer equation to (101) –located at 2θ=7.94°- and (011) –located at 2θ=7.95°- reflections) and TEM micrographs of the sample confirm the formation of nanometer-size particle with an average size of 52 nm (Figure 2). Moreover, DLS analysis of an aqueous suspension of the zeolite nanoparticles indicates a very moderate degree of aggregation of the zeolite nanoparticles with a monomodal distribution centered at an hydrodynamic diameter of 74 nm, consistent with the size of the particles estimated by TEM (see Figure SI-1-A for DLS curve). The good crystallinity of the sample is preserved after calcination (curve (b) on Figure 1). The overall modification of the diffractogram between uncalcined and calcined sample is not only due to the elimination of the template from the porosity (which modifies the relative intensities of the diffraction peaks), but also to a well-documented change in the crystal symmetry, from orthorhombic before calcination (space group Pnma) to monoclinic after (space group $P12_1/m1$, ICDD file 00-044-0003) [15]. Compared to the uncalcined sample, the bump, that is indicative of the presence of an amorphous phase, increases slightly but remains weak, and the size of the

crystalline domains (Scherrer equation applied to the (011) –located at 2θ=7.93°- reflection) is almost unchanged (36 nm).

The nanometer size of the zeolite particles is further supported by the textural properties (N_2-sorption) of the zeolite nanoparticles (orange curve of Figure SI-1-B). The high BET surface area (633 $m^2.g^{-1}$, Table 2) compared to that of conventional ZSM-5 zeolite (ca. 480 $m^2.g^{-1}$) is associated to the presence of an additional porosity. Indeed the surface area associated with micropores (pores smaller than 2 nm) accounts for 488 $m^2.g^{-1}$, and a significant part of the surface is associated with small mesopores (between 2 and 5 nm, 89 $m^2.g^{-1}$) and large mesopores/external surface (pores larger than 5 nm, 56 $m^2.g^{-1}$).

3.2. γ-Al_2O_3 and ZrO_2 based composites

As detailed in the experimental part, composites were prepared by adding, at the start of the hydrothermal treatment, the support material in the solution containing the zeolite precursors. Compositions and textural properties of the composites are reported in Table 2.

The XRD pattern of the γ-Al_2O_3 based composite obtained after 60 h hydrothermal treatment is similar to the one of the starting γ-Al_2O_3 and do not show any sign of the presence of ZSM-5 crystallites (Figure SI-2). Nevertheless, the sample contains SiO_2 (15 wt%, compared to 46 wt% if the extent of zeolite crystallisation was the same as in the reference bottle). Prolonging the hydrothermal treatment to 100 h do not bring any change in the diffractogram.

For the ZrO_2 support, after a hydrothermal treatment of 60 h, beside the reflections associated with the ZrO_2 monoclinic phase (ICDD 00-037-1484) a very weak signal can be observed at 2θ = 23.17° which corresponds to the position of the most intense reflection of the ZSM-5 structure ((501) reflection). In order to further investigate the crystallization of ZSM-5 nanoparticles in presence of zirconia the hydrothermal treatment was prolonged to 100 h. The reflections of the ZSM-5 structure are clearly visible on the XRD pattern of the obtained sample (Figure 3) and the size of the zeolite domains can be estimated at 36 nm (Scherrer

equation applied to the peak associated with the (501) reflection). Moreover, the measured 43 wt% of SiO_2 (Table 2) in this sample corresponds to the maximum possible SiO_2 content based on the initial composition, and is much higher than the 8 wt % for a 60 h hydrothermal treatment.

These samples were further characterized using N_2-sorption. Their surface areas are reported in Table 2 ~~(surface areas of the corresponding support are reported in Table 1)~~. The surface area of the γ-Al_2O_3 based composite, is slightly lower than the one of the starting γ-Al_2O_3 and with no significant contribution from microporosity. The surface area of the silica-rich component can be roughly evaluated to 50 $m^2\ g^{-1}$ (based on the SiO_2 content and assuming that the surface area of the γ-Al_2O_3 component is preserved). This relatively low surface area is consistent with the absence of a zeolite phase. The good crystallinity of the ZSM-5 in the ZrO_2-based composite obtained after 100 h hydrothermal treatment is preserved after calcination (Figure SI-3), and the surface area of this sample significantly higher than that of the ZrO_2 support. Moreover, microporosity contributes for a large part to this increase of surface area. The surface area of the SiO_2-rich component can be estimated at 358 $m^2\ g^{-1}$. This value, although high, is still almost two times lower than the specific surface area the ZSM-5 nanoparticles, 640 $m^2\ g^{-1}$. Hence, the silica-rich phase is probably only partially crystallized as ZSM-5.

TEM micrographs of the composite samples are shown on Figure 4 (TEM micrographs of the ZrO_2 and Al_2O_3 supports are reported as supporting information on Figure SI-4). On the micrograph of the alumina-based composite, the characteristic platelet shape of the γ-Al_2O_3 nanoparticles is clearly visible but there is no evidence of the formation of segregated silicarich particles. A closer look to the micrographs reveals a thin layer (5-10 nm) embedding the alumina particles, that can be assigned to a silica-rich coating. On the micrograph of the zirconia-based composite, two components can also be distinguished: (i) light gray almost spherical particles with a rough surface and whose diameter is about 50 nm, corresponding to the (pseudo)zeolite nanoparticles and, (ii) smaller (20-30 nm) darker particles of irregular shape and smooth surface, corresponding to the zirconia support. Although the intimacy

between the two components seems good, there is no definitive evidence of a nucleation of the zeolite particles on the zirconia support.

3.3. CNT based composites

The XRD pattern of the ZSM-5/CNT sample (Figure 5b), clearly indicates the presence of a high fraction of well-crystallized zeolite nanoparticles in this sample. The size of the crystalline domains (Scherrer equation applied to the (501) reflection) is about 32 nm. The composition of the composite before calcination can be estimated based on the TGA curve (see Figure SI-5). Two separate weight losses can be observed, a first one between RT and 500°C and a second one between 500 and 700°C. The weight loss occurring between 500 and 700°C (high temperature weight loss, ca. 28 %) can be assigned, by comparison with the TGA curve of CNT to the decomposition of the CNT, while the weight loss occurring at lower temperature (low temperature weight loss, 31%) can be assigned to the decomposition/desorption of organic molecules (TPA^+ molecules present in the pores of the zeolite and adsorbed in excess on the surface of the composite) and of water. Finally, the fraction remaining after thermal treatment at 900°C (41%) can be assigned to the inorganic part of the composite. Hence, the fraction of CNT in the composite is about 28% and the fraction of zeolite-like component (excluding the contribution of the template) about 41%. The fraction of zeolite in the uncalcined composite is lower than could be expected based on the composition of the synthesis solution. This indicates that the crystallization of the zeolite is only partial (yield of about 24% based on silica) and/or that a significant fraction of the zeolite nanoparticles formed during the synthesis remained in suspension during the centrifugation step because they were not attached to the CNT. This TGA curve was also be used to estimate the fraction of zeolite after calcination at 500°C (41/(28+41)=58%, Table 2).

ZSM-5/CNT composite was calcined at 500°C (instead of 550°C for the other composites) in order to limit the thermal decomposition of the CNT. The shape of the N_2-sorption isotherm of the composite (See Figure SI-1-B) is characteristic of the presence of both micropores and mesopores/external surface. The surface area of the composite, 776 $m^2\,g^{-1}$, exceeds

significantly the weighted average of the surfaces of its CNT (392 $m^2.g^{-1}$, 41%, Table 2) and zeolite (633 $m^2.g^{-1}$, 59%, Table 2) components (534 $m^2.g^{-1}$), with a high fraction of "open" surface (about 1/3 of the surface is associated with pores larger than 5 nm). This, by itself is a good indication of the formation of a composite material.

The presence of the zeolite nanoparticles and the CNT and their close intimacy is evidenced by the TEM micrograph of the ZSM-5/CNT (Figure 6 a&b). To further investigate the nature of the ZSM-5/CNT composite, the TEM micrograph of the same sample but after calcination at 700 °C (to fully decompose the CNT while leaving the zeolite component) is also shown for comparison (Figures 6 c&d). Beside the zeolite nanoparticles, "ghost" nanotubes are present. We checked that this ghost structure is absent when the carbon nanotubes alone are calcined at 700°C. Hence, these tubes are silica-based and their presence indicates that the hydrothermal treatment leads not only to the formation of the zeolite nanoparticles but also to a coating of the carbon nanotubes by a silica-like materials. The exact nature of these nanotubes (zeolite, amorphous silica or something in between) remains uncertain.

4. Discussion

This study clearly establishes that different supports have a different impact on the formation of ZSM-5 nanoparticles: in presence of γ-Al_2O_3 particles, crystallization of the ZSM-5 nanoparticles is completely inhibited; in presence of ZrO_2 particles, crystallization of ZSM-5 is slowed down and ZSM-5 crystallites are clearly observed only after extending the duration of the hydrothermal treatment (100 h instead of 60 h). Finally, in presence of carbon nanotubes, crystallization is not delayed and a good interaction between the zeolite and the carbon nanotube is observed.

The negative impact of a too high Al concentration on the kinetic of crystallization of ZSM-5 particles using conventional synthesis protocols has been clearly established [16]. Hence, inhibition in the crystallization of the ZSM-5 nanoparticles in presence of alumina could be due to alumina dissolution in the temperature and pH conditions necessary to the

crystallization of the ZSM-5 nanoparticles. Indeed, alumina undergo, in water, a weathering that is temperature [17] and pH [18] dependent and the amount of dissolved Al can reach relatively high values [19]. Alumina dissolution leads usually to the formation of boehmite or bayerite crystals that could not be observed in the present experiments. In the present work, the absence of detectable aluminum (oxo)hydroxide phases is likely related to the presence of silicon species that lead to the formation of aluminosilicate complexes [20].

To investigate a possible relation between the presence of dissolved aluminum species and the absence of crystallization of colloidal ZSM-5 nanoparticles, we have attempted to prepare (unsupported) ZSM-5 nanoparticles in presence of increasing concentrations of aluminum. We have observed that, when the Si/Al ratio in the solution is decreased, the crystallization of the ZSM-5 particles in strongly inhibited. For example, a yield of 50% is obtained after 50 h for a Si/Al ratio of 100. For a Si/Al ratio of 55, reaching a similar yield (45%) requires 108 h (and 156 h for a Si/Al ratio of 40). Moreover, when Si/Al reaches 30, the crystallization of ZSM-5 could not be observed, even after increasing the duration of the hydrothermal treatment to 360 h and the temperature to 80 °C. Yields and main characteristics of the ZSM-5 nanoparticles obtained during this series of experiments are reported in Table S1.

These results confirm that the inhibition of ZSM-5 crystallization in presence of γ-Al_2O_3 support is indeed due to the partial dissolution of γ-Al_2O_3 that leads to a too high concentration of dissolved aluminum species. It is important to emphasize here that inhibition of crystallization in presence of γ-Al_2O_3 is also related the choice of the zeolite structure and will likely not occur for zeolites that can be prepared in presence of high concentration of dissolved aluminum (e.g. beta zeolite). To prepare ZSM-5/γ-Al_2O_3 nanocomposites other experimental approaches should be preferred such as heterocoagulation that takes advantage of the large difference in the points of zero charge of zeolite and boehmite (aluminum oxihydroxide, precursor of γ-Al_2O_3) [6].

For the ZSM-5/ZrO_2 composites, the presence of the ZrO_2 particles in the solution has a moderate inhibiting effect on the growth of the zeolite. This is also likely due to the presence of dissolved Zr species. Indeed, Wang et al. observed that the crystallization of Zr-ZSM-5

(with Zr atoms in tetrahedral substitution in the MFI framework) is slowed down when the Zr concentration is increased and that the formation of Zr-ZSM-5 was difficult at too high Zr/Si ratio [21]. The fact that, at variance with γ-Al_2O_3, ZSM-5 crystallization is still possible in presence of ZrO_2 is probably due to the lower solubility or ZrO_2 in the conditions used for the synthesis of ZSM-5 [17-19, 22]. Although the composite is quite homogeneous, examination of the TEM micrograph does not show any clear evidence of a growth of the zeolite phase on the surface of the ZrO_2 nanoparticles. Hence, ZSM-5 particles are likely formed in solution and the composite is produced afterwards by heterocoagulation of the two oxides. The absence of nucleation of Zeolite NPs at the surface of the ZrO_2 particle could be due to the relatively low PZC of ZrO_2 (PZC=5.5), leading to a highly negatively charged surface in the condition of zeolite synthesis.

The CNT is the support that led to the most promising results. Indeed, thanks to its chemical neutrality (the addition of this support does not modify the composition of the zeolite nucleation solution), the kinetic of nucleation of the zeolite nanoparticles is almost unchanged in presence of CNT (as mentioned above, the yield in zeolite could possibly be moderately reduced). The formation of a composite is also supported by the TEM images and the analysis of the N_2-sorption isotherm. Nevertheless, even for this support, the pre-existence of the solid-liquid interface does not seem to favor the formation of the zeolite nanoparticles and, based on the TEM images for this sample, one cannot conclude unambiguously that the nucleation of the zeolite nanoparticles took place mostly/only at the surface of the CNT. Indeed, even if the zeolite nanoparticles seem to be anchored on the CNT, their nucleation could have occurred in solution followed by their attachment to the CNT surface. The thin silicon-based coating that covers the CNT (evidenced by the TEM images of the sample calcined at 700°C) could favor the anchoring of these preformed zeolite NPs on the CNT surface.

5. Conclusion

The three families of supports tested in this work have shown quite different behaviors toward the formation of zeolite-based composites and these differences can be rationalized based on their different chemical properties: the suppressed crystallization of ZSM-5 nanoparticles in presence of alumina support is likely due to the high reactivity of γ-Al_2O_3 in hydrothermal conditions that modifies sensibly the aluminum concentration in the solution. Zirconia, plays a similar role but to a lower extent and delays significantly the nucleation of ZSM-5 compared to the reference support-free synthesis. Moreover, Zeolite NPs do not seem to nucleate at the surface of the ZrO_2 support. With carbon nanotubes (CNT), a non-reactive support, zeolite nucleation is not delayed and a thin silicon-rich coating is also formed on the surface of the CNT. N_2-sorption and TEM indicate the formation of a zeolite/CNT nanocomposite.

Even if nucleation of ZSM-5 nanoparticles on zirconia and alumina was not possible in the conditions explored in this study, a direct formation of supported zeolite nanoparticles is probably possible, for example with other types of zeolites that would be less sensitive to the modification of the composition of the solution by dissolution of the support, such as beta zeolites NPs.

Declarations of interest:

None.

Acknowledgments

This work was supported by French state funds managed by the ANR within the ‘‘Investissements d’Avenir’’ program (reference ANR-11-IDEX-0004-02) and more specifically within the frame-work of the Cluster of Excellence MATISSE.

References

[1] J. Perez-Ramirez, C.H. Christensen, K. Egeblad, C.H. Christensen, J.C. Groen, Hierarchical zeolites: enhanced utilisation of microporous crystals in catalysis by advances in materials design, Chemical Society Reviews, 37 (2008) 2530-2542.
[2] S. Mintova, J. Grand, V. Valtchev, Nanosized zeolites: Quo Vadis?, Comptes Rendus Chimie, 19 (2016) 183-191.
[3] G.-T. Vuong, V.-T. Hoang, D.-T. Nguyen, T.-O. Do, Synthesis of nanozeolites and nanozeolite-based FCC catalysts, and their catalytic activity in gas oil cracking reaction, Applied Catalysis A: General, 382 (2010) 231-239.
[4] P.M. Lima, C.V. Gonçalves, C.L. Cavalcante Jr, D. Cardoso, Sorption kinetics of linear paraffins in zeolite BEA nanocrystals, Microporous and Mesoporous Materials, 116 (2008) 352-357.
[5] N. Batalha, S. Morisset, L. Pinard, I. Maupin, J.L. Lemberton, F. Lemos, Y. Pouilloux, BEA zeolite nanocrystals dispersed over alumina for n-hexadecane hydroisomerization, Microporous and Mesoporous Materials, 166 (2013) 161-166.
[6] O. Ben Moussa, L. Tinat, X. Jin, W. Baaziz, O. Durupthy, C. Sayag, J. Blanchard, Heteroaggregation and Selective Deposition for the Fine Design of Nanoarchitectured Bifunctional Catalysts: Application to Hydroisomerization, ACS Catalysis, 8 (2018) 6071-6078.
[7] V. Mavrodinova, M. Popova, V. Valchev, R. Nickolov, C. Minchev, Beta zeolite colloidal nanocrystals supported on mesoporous MCM-41, Journal of Colloid and Interface Science, 286 (2005) 268-273.
[8] J. Zecevic, G. Vanbutsele, K.P. de Jong, J.A. Martens, Nanoscale intimacy in bifunctional catalysts for selective conversion of hydrocarbons, Nature, 528 (2015) 245-248.
[9] N. Rangnekar, N. Mittal, B. Elyassi, J. Caro, M. Tsapatsis, Zeolite membranes – a review and comparison with MOFs, Chemical Society Reviews, 44 (2015) 7128-7154.
[10] N. Batalha, L. Pinard, Y. Pouilloux, M. Guisnet, Bifunctional Hydrogenating/Acid Catalysis: Quantification of the Intimacy Criterion, Catalysis Letters, 143 (2013) 587-591.
[11] Z. Wang, M.A. Al-Daous, E.R. Kiesel, F. Li, A. Stein, Design and synthesis of 3D ordered macroporous ZrO2/Zeolite nanocomposites, Microporous and Mesoporous Materials, 120 (2009) 351-358.
[12] C.-Y. Hsu, A.S.T. Chiang, R. Selvin, R.W. Thompson, Rapid Synthesis of MFI Zeolite Nanocrystals, The Journal of Physical Chemistry B, 109 (2005) 18804-18814.
[13] R. Selvin, A.S.T. Chiang, Some Observations on the Synthesis of Fully-Dispersible Nanocrystalline Zeolite ZSM-5, Journal of Nanoscience and Nanotechnology, 14 (2014) 7351-7359.
[14] R. Selvin, H.-L. Hsu, L.S. Roselin, M. Bououdina, Effect of Aging on the Precursor Sol for the Synthesis of Nanocrystalline ZSM-5, Synthesis and Reactivity in Inorganic, Metal-Organic, and Nano-Metal Chemistry, 41 (2011) 1028-1032.

[15] E.L. Wu, S.L. Lawton, D.H. Olson, A.C. Rohrman, G.T. Kokotailo, ZSM-5-type materials. Factors affecting crystal symmetry, The Journal of Physical Chemistry, 83 (1979) 2777-2781.
[16] D.B. Shukla, V.P. Pandya, F. Fetting, Study of ZSM-5 zeolite crystallization: influence of reagents on the crystallization of (NH4-TPA)-ZSM-5 zeolites, Materials Chemistry and Physics, 33 (1993) 50-57.
[17] G. Lefèvre, M. Duc, P. Lepeut, R. Caplain, M. Fédoroff, Hydration of γ-Alumina in Water and Its Effects on Surface Reactivity, Langmuir, 18 (2002) 7530-7537.
[18] X. Carrier, E. Marceau, J.-F. Lambert, M. Che, Transformations of γ-alumina in aqueous suspensions: 1. Alumina chemical weathering studied as a function of pH, Journal of Colloid and Interface Science, 308 (2007) 429-437.
[19] G. Verdes, R. Gout, S. Castet, Thermodynamic properties of the aluminate ion and of bayerite, boehmite, diaspore and gibbsite, European journal of mineralogy, 4 (1992) 767-792.
[20] R. Gout, G.S. Pokrovski, J. Schott, A. Zwick, Raman spectroscopic study of aluminum silicate complexes at 20 C in basic solutions, Journal of solution chemistry, 29 (2000) 1173-1186.
[21] G.-R. Wang, X.-Q. Wang, X.-S. Wang, S.-X. Yu, Synthesis and catalytic Reaction of [Zr] ZSM-5, in: T. Hattori, T. Yashima (Eds.) Studies in Surface Science and Catalysis, Elsevier1994, pp. 67-74.
[22] S.N. Lvov, X.Y. Zhou, G.C. Ulmer, H.L. Barnes, D.D. Macdonald, S.M. Ulyanov, L.G. Benning, D.E. Grandstaff, M. Manna, E. Vicenzi, Progress on yttria-stabilized zirconia sensors for hydrothermal pH measurements, Chemical Geology, 198 (2003) 141-162.

Table 1: Surface area (external surface is also reported between parentheses) and the amount of each support added to the zeolite precursor suspension

	γ-Al_2O_3	**ZrO_2**	**CNT**
S_{BET} [S_{ext}] ($m^2.g^{-1}$)	84 [46]	22 [10]	237 [121]
weight (g)	0.80	3.3	0.29

Table 2: Main characteristics of the composites

	wt% "zeolite"	Total Surface Area ($m^2.g^{-1}$)	Surface area ($m^2.g^{-1}$) for pores	
			<2nm[(d)]	> 5 nm[(d)]
ZSM-5	100	633	488	56
CNT-500	0	392[(c)]	33	132
γ-Al_2O_3	0	84	0	46
ZrO_2	0	22	0	10
ZSM-5/γ-Al_2O_3	15[(a)]	79	24	25
ZSM-5/ZrO_2(60h)	8[(a)]	49	27	15
ZSM-5/ZrO_2(100h)	43[(a)]	166	136	20
ZSM-5/CNT	59[(b)]	776	345	255

[(a)] wt% of zeolite estimated from chemical analysis by XRF based on the fraction of SiO_2 [(b)] wt% of zeolite estimated from weight loss upon calcination and taking into consideration the weight loss associated with the zeolite template (TGA analysis) [(c)]surface area of the CNT increases upon calcination at 500°C under air from 237 to 392 $m^2.g^{-1}$ due to a partial decomposition of the CNT upon calcination. Surface area for pores < 2nm and > 5nm were calculated from NLDFT analysis of adsorption isotherm.

Figure 1: X-ray diffractograms of the ZSM-5 nanoparticles (a) before (ICDD 01-085-1208) and (b) after (ICDD 00- 044-0003) calcination.

Figure 2: TEM micrograph of ZSM-5 nanoparticles (uncalcined)

Figure 3: X-ray diffractograms of the ZrO_2-based composites: (b) after an hydrothermal treatment of 60h; (c) after an hydrothermal treatment of 100h; (the diffractograms of the ZrO_2 support (curve (a) and of the zeolite nanoparticles (unsupported), curve (d) are also shown for comparison); the left part of the figure shows a zoom in the 2θ range 23 to 27°.

Figure 4: TEM micrographs of: (a) ZSM-5/Al_2O_3 (insert at the right-bottom corner corresponds to a larger magnification micrograph) and, (b) ZSM-5/ZrO_2 composites.

Figure 5: X-ray diffractograms of: (a) CNT, (b) ZSM-5/CNT-uncalcined, (c) ZSM-5/CNT calcined and (d) ZSM-5 calcined.

Figure 6: TEM micrographs of the ZSM-5/CNT composite: (a) & (b): after calcination at 500°C ((a) general view; (b) enlarged image); (c) & (d): after calcination at 700°C ((c) general view; (d) enlarged image).

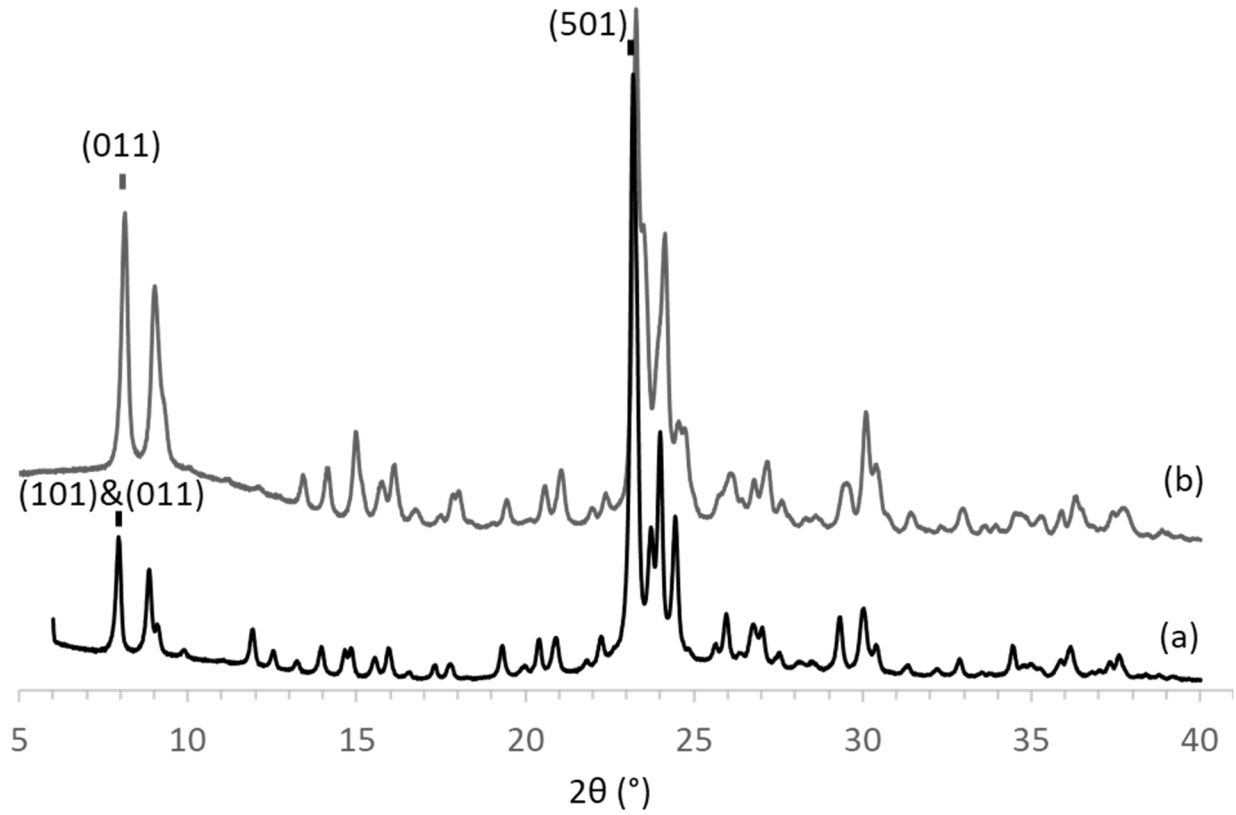

Figure 1: X-ray diffractograms of the ZSM-5 nanoparticles (a) before (ICDD 01-085-1208) and (b) after (ICDD 00- 044-0003) calcination.

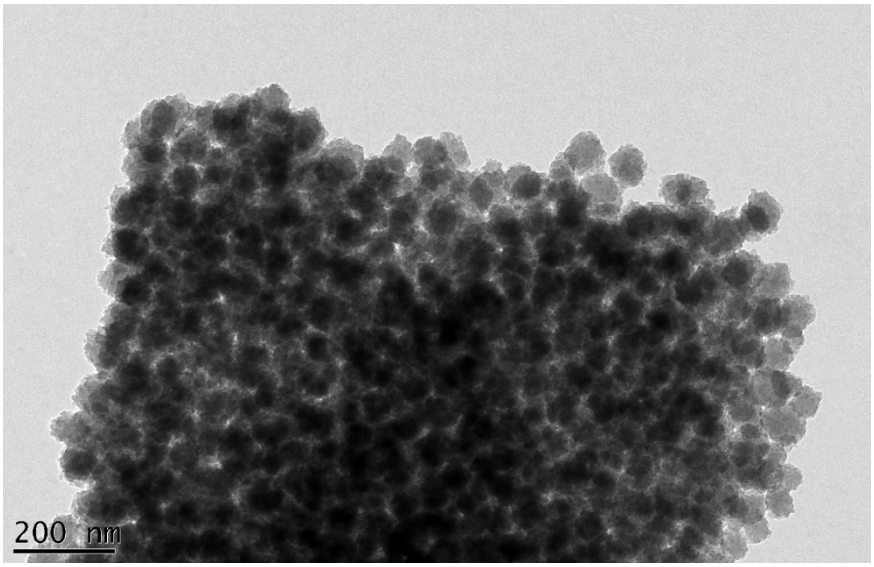

Figure 2: TEM micrograph of ZSM-5 nanoparticles (uncalcined)

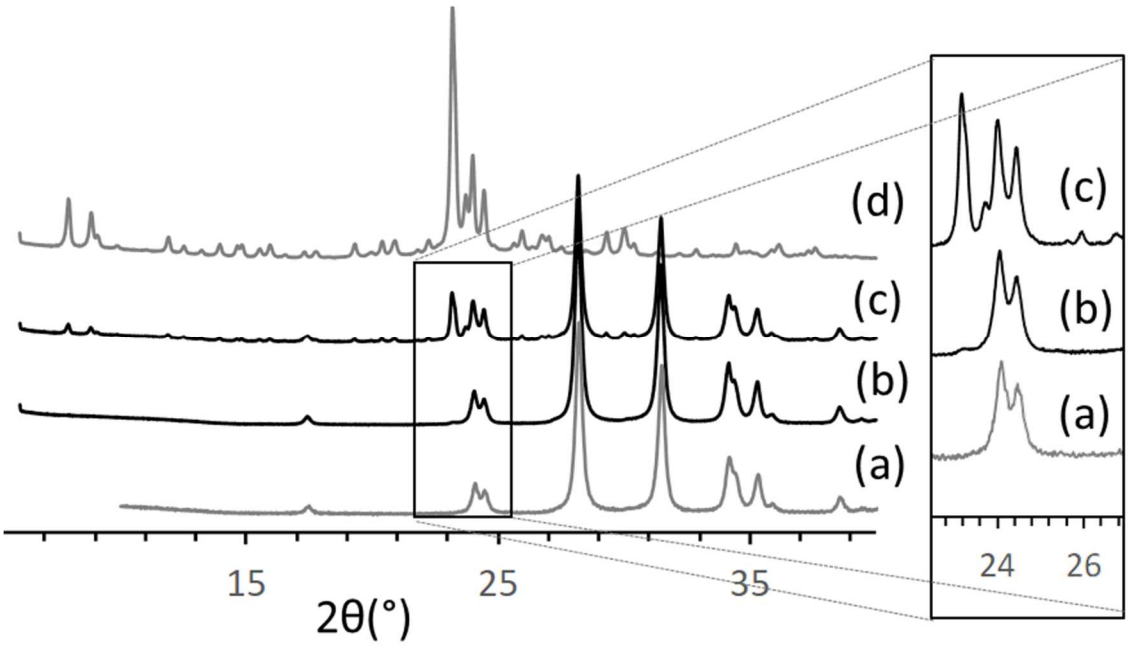

Figure 3: X-ray diffractograms of the ZrO_2-based composites : (b) after an hydrothermal treatment of 60h; (c) after an hydrothermal treatment of 100h; (the diffractograms of the ZrO_2 support (curve (a) and of the zeolite nanoparticles (unsupported), curve (d) are also shown for comparison); the left part of the figure shows a zoom between 2θ=23 & 27°.

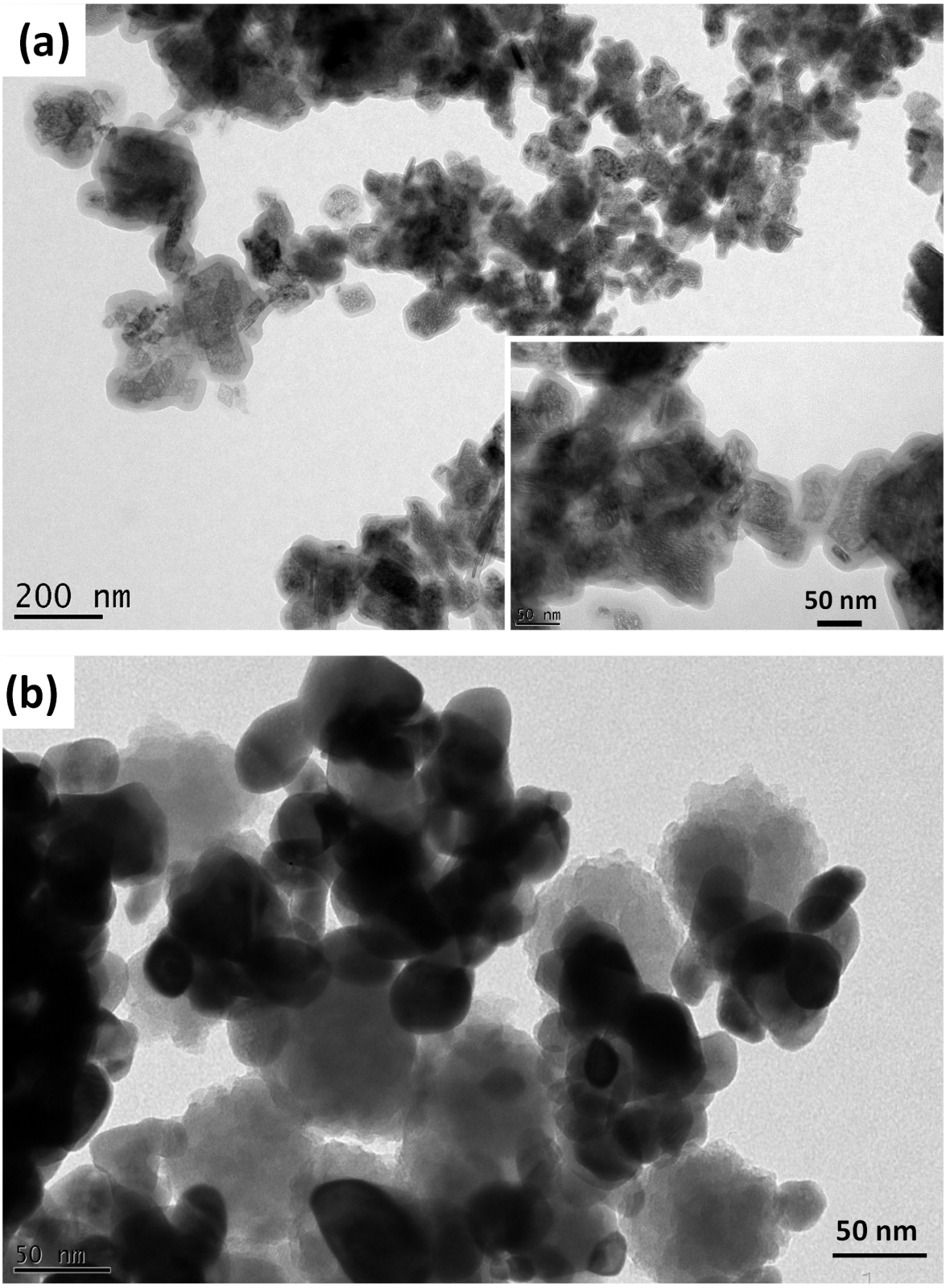

Figure 4: TEM micrographs of: (a) ZSM-5/Al_2O_3 (insert at the right-bottom corner corresponds to a larger magnification micrograph) and, (b) ZSM-5/ZrO_2 composites.

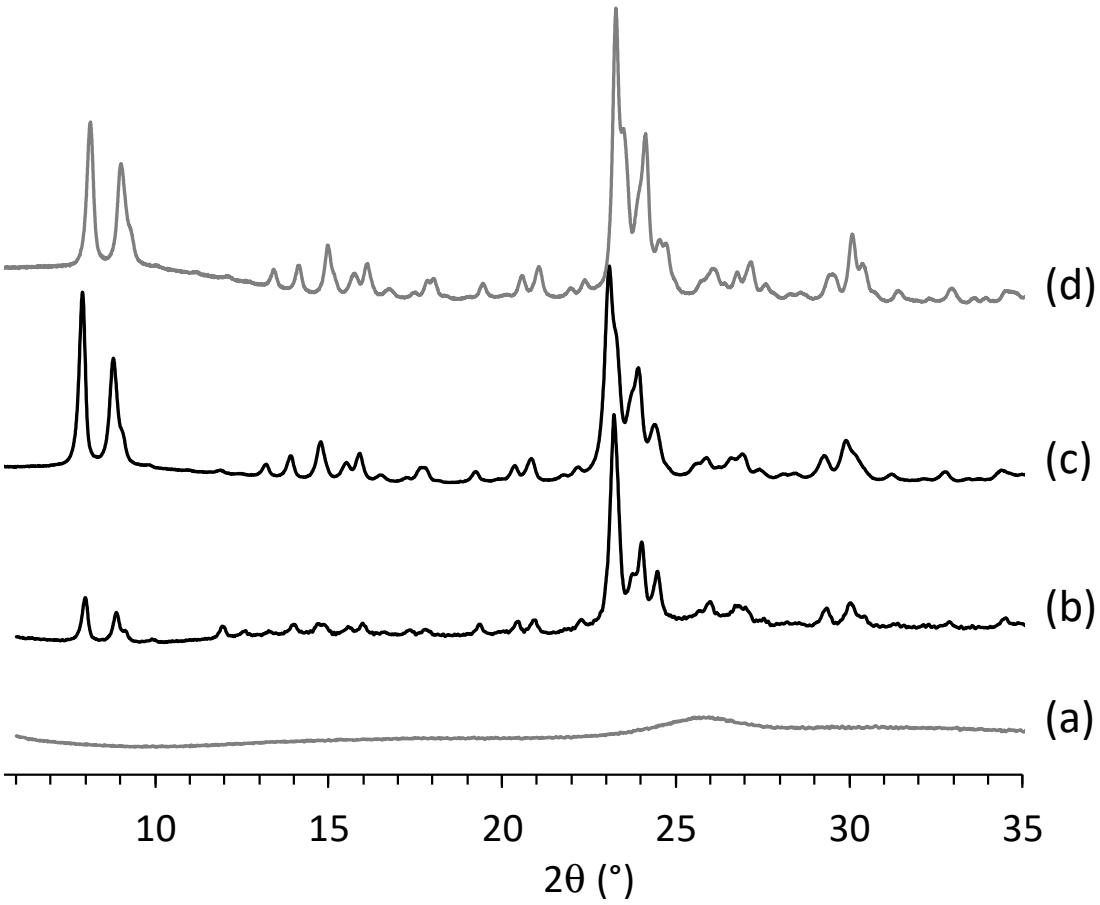

Figure 5: X-ray diffractograms of: (a) CNT, (b) ZSM-5/CNT-uncalcined, (c) ZSM-5/CNT calcined and (d) ZSM-5 calcined.

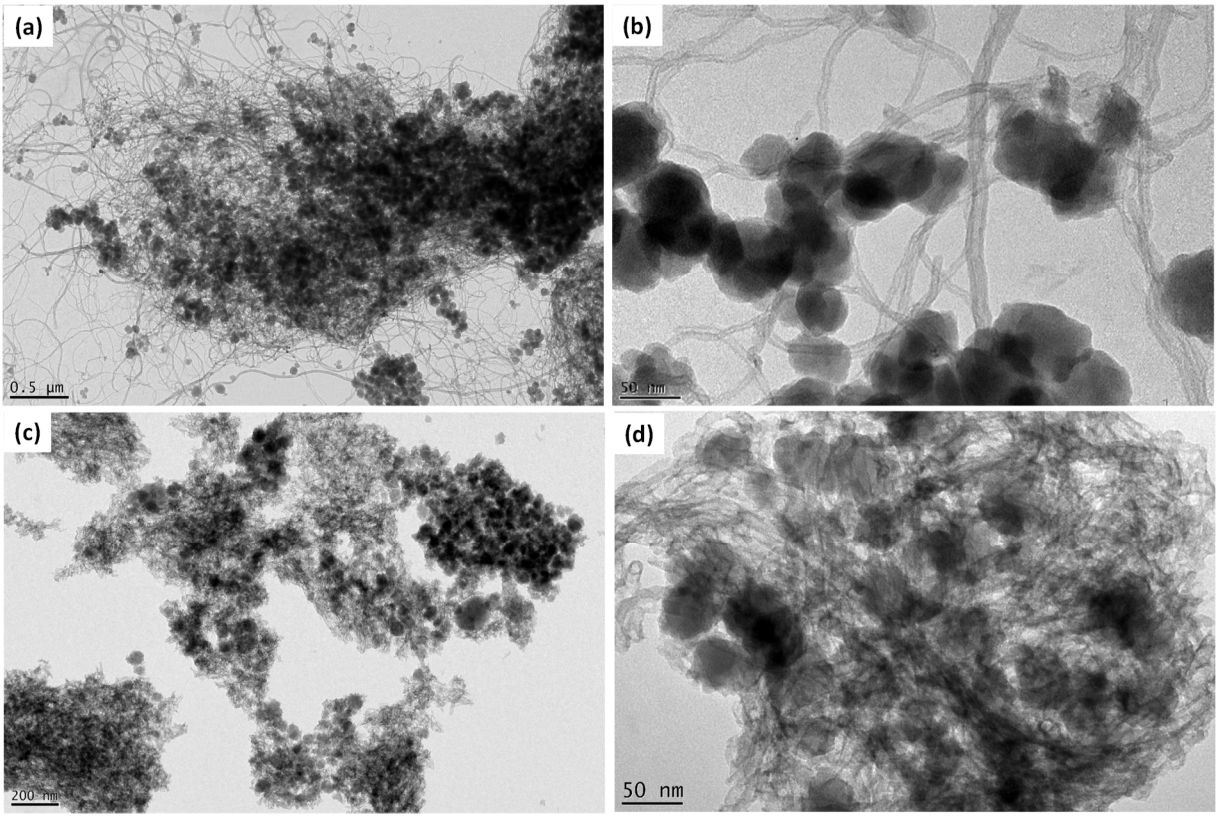

Figure 6: TEM micrographs of the ZSM-5/CNT composite: (a) & (b): after calcination at 500°C ((a) general view; (b) enlarged image); (c) & (d): after calcination at 700°C ((c) general view; (d) enlarged image).